An analytical model of wave bottom boundary layers incorporating turbulent relaxation and diffusion effects

An Analytical Model of Wave Bottom Boundary Layers Incorporating Turbulent Relaxation and Diffusion Effects

QINGPING ZOU

Department of Oceanography, Dalhousie University, Halifax, Nova Scotia, Canada

ABSTRACT

To calculate the effects of turbulent relaxation on oscillatory turbulent boundary layers, a viscoelastic term is added to an eddy viscosity model. The viscoelastic term parameterizes the lag of turbulent properties in response to imposed oscillatory shear and is proportional to the ratio between the timescales of eddy dissipation and of the oscillating flow. It is found that the turbulent relaxation plays an important role in the phase variations of velocity and shear stress with elevation, and that it decreases the friction factor and the phase lead of bed shear stress over free stream velocity.

To assess the effects of turbulent diffusion in this problem, the viscoelastic model is extended by further introducing a turbulent diffusion term in the model. The comparisons between these two models indicate that turbulent diffusion significantly reduces the magnitudes of shear stress and velocity perturbation in the outer region of the boundary layer. It is also found that the effects of turbulent relaxation and diffusion increase with increasing relative roughness. As a result, the analytical solutions demonstrate an overall improvement over the eddy viscosity model in predicting the observed temporal evolution of velocity and shear stress profiles; this improvement is more distinct for rough beds than smooth beds.

1. Introduction

Shallow water waves and tidal flows generate an oscillatory boundary layer at the ocean bottom that is often very thin compared to the water depth. This problem is significant to our understanding of coastal processes such as wave energy dissipation (cf. Weber 1991; Tolman 1994; Young and Gorman 1995; Agrawal et al. 1992), sediment transport, and suspension (Nielsen 1992; Fredsoe and Deigaard 1992). Quantitative evaluation of velocity fields, shear stress, drag force, and mass transport within the layer depends on the Reynolds closure models used in solving the Reynolds-averaged Navier–Stokes equation (see Sleath 1990 for review and Grant and Madsen 1986 for background knowledge). Among these models, only the relatively primitive eddy viscosity models have yielded analytical solutions (Kajiura 1968; Johns 1969; Grant 1977; Smith 1977; Brevik 1981; Myrhaug 1982; Lavelle and Mofjeld 1983; Trowbridge and Madsen 1984; Davies 1986; Madsen and Wikramanayake 1991). In fact, the analytical tractability and comparative simplicity of eddy viscosity models

have resulted in their prominence and widespread application.

Nonetheless, these models neglect turbulent relaxation or vertical diffusion effects; therefore, none of them allow the phase of the eddy viscosity to change with height above the bed (cf. Davies 1986). These effects are included in the second-order turbulent closure models (cf. Sleath 1990; Fredsoe and Deigaard 1992) and their solutions, however, have to be evaluated numerically; therefore, they are hard to interpret and far less accessible than their analytical counterparts. As a compromise between these two types of model, we approach this problem differently by using a viscoelastic model that includes the most important aspects of the second-order closure models, yet is simple enough to yield analytical solutions in a closed form. The reader should refer to Speziale (1991) for a review on Reynolds-stress closures in steady turbulent flow and Hanjalic (1994) and Brereton and Mankbadi (1995) for a review of the treatment of unsteady turbulent flow.

Measurements of suspended sediment in tidal flows indicate a lag in concentration behind the free stream velocity and the bed shear stress (cf. Davies 1977; Dyer 1986). It is also observed that, at any level, the suspended sediment concentration is higher within a decelerating current than that within an accelerating cur-

Corresponding author address: Dr. Qingping Zou, Department of Oceanography, Dalhousie University, Halifax, NS B3H-4J1, Canada. E-mail: qingping.zou@dal.ca

rent. During their measurements of sediment suspension under wave groups, Hay and Bowen (1994) noticed a lag between the sediment concentration and wave group envelope that increases with the distance from the bed. From their measurements of bottom turbulent layers induced by tidal flows, both Gordon (1974) and McLean (1983) found that shear stress and turbulent kinetic energy are larger during the decelerating phase of the flow than those during the accelerating phase. The hysteresis of sediment concentration is a consequence of the hysteresis of shear stress and turbulent kinetic energy combined with the nonzero fall velocity of the sediment. It has also been found that, away from the bottom, shear stress lags the free stream velocity and that maximum bedload sediment transport occurs before the maximum free stream velocity and shear stress aloft (cf. Lavelle and Mofjeld 1983).

These field measurements suggest that the phase lead of shear stress over free stream velocity decreases from a positive value at the bed to a negative value away from the bed. In laboratory studies of oscillating flow, Sleath (1987) observed a 180° phase shift in shear stress between the bed and a certain height above. He suggested that it is caused by the jets of fluid associated with vortex formation and ejection in oscillatory flow over rough beds. It is obvious that such a proposal does not apply to the wave boundary layer over smooth beds where a similar phenomenon was observed by Jensen et al. (1989). In contrast, from the comparison of the present viscoelastic model with observations, we draw the conclusion that eddy relaxation is the mechanism behind this behavior.

The theoretical studies of oscillatory turbulent boundary layer prior to the 1980s were prevailed by the time-invariant eddy viscosity models of different forms. They were proposed initially by analogy with the steady turbulent flow. Experimental studies of oscillatory turbulent flow have been mostly mean (ensemble average) flow measurements (cf. Jonsson and Carlsen 1976; Van Doorn 1982). As a result, few theoretical studies of this problem are able to justify their predictions of Reynolds stresses by comparison with direct measurements. Sleath's (1987) and Jensen et al.'s (1989) measurements complement each other and provide a comprehensive dataset of turbulence properties in addition to the mean flow.

From his analysis of Jonsson and Carlsen's (1976) experiment, Nielsen (1985) observed a phase shift between shear stress and velocity gradient that varies with height above the bed. He suggested that either a time-variant real eddy viscosity or a complex eddy viscosity be adapted to explain such behavior. Meanwhile, he pointed out the lack of a theoretical basis for the complex eddy viscosity. As shown later in this presentation, introducing a turbulent relaxation term to the conventional eddy viscosity model leads to a complex eddy viscosity and results in an improved prediction of the observed velocity profiles of Jonsson and Carlsen (1976) and others.

Different from their predecessors, each of Lavelle and Mofjeld (1983), Trowbridge and Madsen (1984), Davies (1986), and Madsen and Wikramanayake (1991) postulated a time-varying eddy viscosity in their study of the wave turbulent boundary. Nevertheless, these models all assume that the time-dependent part of eddy viscosity has the same vertical structure as the steady part, therefore, the phase of eddy viscosity does not vary with height above the bed. This assumption, which contradicts the existing observations and the numerical results provided by the second-order turbulent closure models, is avoided in the present investigation of this problem.

It takes time for the turbulent properties, represented by Reynolds stresses, to relax to attain a new equilibrium state set by a new mean velocity strain at each instant. The lag depends on the ratio between the time scales of eddy relaxation and of the oscillating shear flow, and therefore varies with height. This relaxation aspect of turbulent flow is not adequately described by any of the eddy viscosity models listed above.

Adding a viscoelastic term to an eddy viscosity model, we obtain the following equation that is analogous to Maxwell's equation for non-Newtonian flow (cf. Zou 1995, 1998); that is,

$$T_e \frac{D\tau}{Dt} + \tau = \tau_0 \equiv \nu_0(u_z + w_x), \qquad (1.1)$$

where τ is the shear stress, τ_0 is the corresponding shear stress in the eddy viscosity model with a Boussinesq viscosity ν_0, $T_e = l_e/(a_1 u_*)$ is the eddy relaxation time, $\tau_0 = u_*^2$ is the peak shear stress at the bed, u_* is the friction velocity, $l_e = \kappa z$ is the eddy mixing length, κ is von Kármán's constant, $a_1 = -\langle u'w' \rangle/q^2$ is the ratio between shear stress $-\langle u'w' \rangle$, turbulent energy q^2 and its empirical value for steady flow is $a_1 = O(\kappa^2)$ (cf. Townsend 1976; Bradshaw et al. 1967), and the subscripts x and z signify partial differentiation hereinafter. Viscoelastic model (1.1) could be derived from Townsend's turbulent energy equation for steady turbulent flow by neglecting the vertical diffusion term (cf. appendix A of Zou 1998). Following many previous investigators of this problem, we will apply it directly to the oscillatory turbulent flow in this problem.

We assume the near-bottom orbital velocity induced by a progressive wave or tidal flow of the form

$$u_\infty = a\omega \exp(i\omega t - ikx) + \text{c.c.}, \qquad (1.2)$$

where a is the excursion amplitude of the orbital motion, ω is the radian frequency, k is the wavenumber, and c.c. is the complex conjugate of the preceding variable and will be omitted hereinafter. The convective term in (1.1) is $O(ka)$, therefore negligible for a small wave slope, the associated shear stress τ has the same (x, t) dependence as the near-bottom orbital velocity (1.2) and (1.1) reduces to a complex effective eddy viscosity

$$\nu = \frac{\nu_0}{1 + i\alpha(z/l)}, \tag{1.3}$$

where $\alpha = \kappa^2/a_1$ is taken as the weight coefficient of eddy relaxation and $l = \kappa u_*/\omega$ is equivalent to the wave boundary layer thickness proposed by previous investigators. In contrast to the eddy viscosity model $\nu = \nu_0 \equiv \kappa u_* z$, both amplitude and phase of the eddy viscosity (1.3) depend on the oscillatory frequency. The phase of the effective eddy viscosity (1.3), $\Phi_\nu = -\arctan(\alpha z/l)$, decreases from zero at the bed to about $-90°$ at the top of wave boundary layer $z/l \rightarrow \infty$, where the shear stress and velocity strain are in quadrature. In the case of $\alpha = 0$, namely in the absence of eddy relaxation, the closure model (1.3) reduces to the eddy viscosity model, $\nu = \nu_0 \equiv \kappa u_* z$. The former approaches the later asymptotically in the region $z \ll l$ where eddies attain a local equilibrium with the ambient mean flow.

As demonstrated later, it is necessary to further include turbulent diffusion in (1.1) to accurately predict the observed rapid decay of shear stress and velocity defect in the outer region of the boundary layer. Assuming the vertical diffusion of turbulent energy is proportional to its gradient with a diffusivity $\nu_0 = \kappa u_* z$, we have (cf. Townsend 1972; Zou's 1998 appendix A)

$$T_e \frac{D\tau}{Dt} + \tau = \nu_0(u_z + w_x) + T_e(\nu_0 \tau_z)_z. \tag{1.4}$$

Similar to the second-order closure models, the viscoelastic–diffusion model (1.4) represents the turbulent energy balance due to production, dissipation, relaxation, and vertical diffusion. Unlike these models, (1.4) can be solved analytically. Furthermore, most previous eddy viscosity models involve a discontinuity in eddy viscosity or its gradient and a preassumption of matching height between adjacent layers. As shown later, by avoiding these physically unrealistic assumptions, (1.4) results in improved predictions of observed velocity and shear stress profiles within the wave bottom boundary layers.

Although eddy relaxation effects in oscillatory turbulent flow have been recognized by some investigators (Lavelle and Mofjeld 1983; Trowbridge and Madsen 1984; Nielsen 1992, etc.), their quantitative evaluation has not been the focus of previous analysis. Our objective is to apply the viscoelastic closure model (1.1) to the Reynolds-averaged Navier–Stokes equation and calculate the effects of eddy relaxation on oscillatory turbulent flow. Further comparison between the viscoelastic–diffusion model (1.4), the viscoelastic model (1.1) and observations allows us to examine the role of turbulent vertical diffusion in this problem. In section 2, we give a detailed discussion of these two models, substitute them into the Reynolds-averaged Navier–Stokes equation, and derive their analytical solutions. The theoretical and experimental results are compared in section 3. Finally, in section 4, the major findings of this study are summarized and discussed.

2. Governing equations and their solutions

We consider here the wave turbulent boundary layer generated by a progressive wave over a flat seabed. We assume that the associated turbulent flow is neutrally stable and fully developed. The x and z components of the Reynolds-averaged Navier–Stokes equations are

$$\frac{Du}{Dt} = -\left\langle \frac{p}{\rho} \right\rangle_x - \langle u'^2 \rangle_x - \langle u'w' \rangle_z, \tag{2.1a}$$

$$\frac{Dw}{Dt} = -\left\langle \frac{p}{\rho} \right\rangle_z - \langle w'^2 \rangle_z - \langle u'w' \rangle_x, \tag{2.1b}$$

where x is positive in the direction of wave propagation, z is positive upward with $z = 0$ at the bed, $u \equiv \langle u \rangle$ and $w \equiv \langle w \rangle$ are the mean velocity components, p is the mean pressure, ρ is the density, u' and w' are randomly fluctuating velocities in the x and z directions, and angle brackets imply a phase average. The order of magnitude estimation of (2.1b) and the mass conservation equation

$$u_x + w_z = 0 \tag{2.2}$$

show that the vertical pressure gradient is $O[(kl)^2]$, hence

$$\left\langle \frac{p}{\rho} \right\rangle_x = \left\langle \frac{p_b}{\rho} \right\rangle_x + O[(kl)^2] = \frac{Du_\infty}{Dt} + O[(kl)^2], \tag{2.3}$$

where the subscript ∞ denotes the variable in the potential flow just outside of the boundary layer and hereinafter. Substituting (2.3) into (2.1a) and omitting terms of $O(ka)$ and $O(kl)$, we have

$$\frac{\partial u}{\partial t} = \frac{\partial u_\infty}{\partial t} + \tau_z. \tag{2.4}$$

a. The viscoelastic model

Nondimensionalized by scalings

$$\left\{ \frac{u - u_\infty}{u_*}, \frac{\tau}{u_*^2}, \frac{u_\infty}{u_*}, \frac{u}{u_*} \right\}$$
$$= \{\bar{u}_d, \bar{\tau}, \bar{u}_\infty, \bar{u}\} \exp(i\omega t - ikx), \tag{2.5a,b,c}$$

and combined with (1.3), the momentum equation (2.4) becomes

$$\frac{d\bar{\tau}}{d\zeta} = i\kappa \bar{u}_d, \tag{2.6a}$$

where

$$\bar{\tau} = \frac{\kappa\zeta}{1 + i\alpha\zeta} \frac{d\bar{u}_d}{d\zeta} \tag{2.6b}$$

and $\zeta = z/l$ is the stretched coordinate.

The boundary conditions follow from the no-slip condition at the bottom and the continuity of velocity at the top of the boundary layer; that is,

$$\overline{u}_d = \begin{cases} -\overline{u}_\infty & \text{at } \zeta \to \zeta_0 \quad\quad (2.7a) \\ 0 & \text{at } \zeta \to \infty, \quad\quad (2.7b) \end{cases}$$

where $\zeta_0 = z_0/l$, z_0 is a roughness length determined by the geometry of the roughness elements on the seabed, along with the flow condition.

Combination of (2.6a) and (2.6b) gives

$$\frac{\zeta}{1 + i\alpha\zeta}\frac{d^2\overline{\tau}}{d\zeta^2} = i\overline{\tau}. \quad\quad (2.8)$$

By introducing a new independent variable

$$\hat{z} = 2i\beta\zeta, \quad\quad (2.9)$$

where

$$\beta = \sqrt{\alpha}, \qu\quad (2.10)$$

we reduce (2.8) to Whittaker's equation [cf. Olver (1974); Abramowitz and Stegun, sec13.1.31],

$$\overline{\tau}_{\hat{z}\hat{z}} + \left[-\frac{1}{4} - \frac{1}{2\beta\hat{z}}\right]\overline{\tau} = 0. \qu\quad (2.11)$$

The solution to (2.11) that vanishes at $|\hat{z}| \to \infty$ is

$$\overline{\tau} = C \exp\left(-\frac{1}{2}\hat{z}\right)\hat{z} U\left(1 + \frac{1}{2\beta}, 2, \hat{z}\right), \qu\quad (2.12)$$

where U is the confluent hypergeometric function and the constant coefficient C is determined by the no-slip boundary condition at the bed, (2.7a) in combination with (2.6a); that is,

$$\overline{u}_d = \frac{1}{i\kappa}\overline{\tau}_\zeta = -\overline{u}_\infty \quad \text{as } \zeta \to \zeta_0. \qu\quad (2.13)$$

Differentiating (2.12) about ζ and combining with (2.13) and (2.9) gives

$$\overline{u} = \overline{u}_\infty\left[1 - \frac{F(\beta, \zeta)}{F(\beta, \zeta_0)}\right], \qu\quad (2.14a)$$

where the function $F(\beta, \zeta)$ is related to the confluent hypergeometric function U by

$$F(\beta, \zeta) = \exp(-i\beta\zeta)\left[i\beta\zeta U\left(1 + \frac{1}{2\beta}, 2, 2i\beta\zeta\right)\right.$$
$$\left. - U\left(\frac{1}{2\beta}, 1, 2i\beta\zeta\right)\right]. \qu\quad (2.14b)$$

Substituting (2.14) into (2.6b), we obtain

$$\overline{\tau} = -i\kappa\overline{u}_\infty[F(\beta, \zeta_0)]^{-1}\zeta$$
$$\times \exp(-i\beta\zeta)U\left(1 + \frac{1}{2\beta}, 2, 2i\beta\zeta\right). \qu\quad (2.15)$$

In appendix a, we show that, as $\beta \to 0$, the eddy relaxation term becomes zero and (2.14a) becomes

$$\overline{u} = \overline{u}_\infty\left(1 - \frac{\text{ker}2\sqrt{\zeta} + i\,\text{kei}2\sqrt{\zeta}}{\text{ker}2\sqrt{\zeta_0} + i\,\text{kei}2\sqrt{\zeta_0}}\right), \qu\quad (2.16)$$

which is identical to solution of the eddy viscosity model, $\nu = \nu_0 \equiv \kappa u_* z$ (cf. Grant and Madsen 1986). It follows that (2.14) and (2.15) are general solutions for the viscoelastic model with an arbitrary relaxation coefficient β.

On the assumption that the roughness length z_0 is much smaller than the wave turbulent boundary layer thickness l, that is, $\zeta_0 = z_0/l \ll 1$, near the surface ($\zeta \to \zeta_0$), u approaches its asymptotic value of

$$\overline{u}(\zeta \to \zeta_0) = \overline{u}_\infty\left\{1 - \frac{\beta + \varphi\left(\frac{1}{2\beta}\right) + 2\gamma + \ln 2i\beta\zeta}{\Gamma\left(\frac{1}{2\beta}\right)F(\beta, \zeta_0)}\right\} = \frac{-\overline{u}_\infty}{\beta + \varphi\left(\frac{1}{2\beta}\right) + 2\gamma + \ln 2i\beta\zeta_0}\ln\frac{\zeta}{\zeta_0}, \qu\quad (2.17a,b)$$

where φ is digamma function and γ is Euler's constant, while $\overline{\tau}$ approaches its asymptotic value of

$$\overline{\tau}_0 = \overline{\tau}(\zeta \to \zeta_0) = \frac{-\kappa\overline{u}_\infty}{\Gamma\left(\frac{1}{2\beta}\right)F(\beta, \zeta_0)}$$

$$= \frac{-\kappa\overline{u}_\infty}{\beta + \varphi\left(\frac{1}{2\beta}\right) + 2\gamma + \ln 2i\beta\zeta_0}, \qu\quad (2.18a,b)$$

which is the bed shear stress. As indicated by (2.17a,b) and (2.18a,b), the near-wall flow exhibits a logarithmic velocity profile and a constant shear stress that depend on the viscoelasticity coefficient β.

The bed shear stress is related to the orbital velocity by

$$\overline{\tau}_0 = \frac{1}{2}f_w|\overline{u}_\infty|\overline{u}_\infty \exp(i\Phi_{\tau_0}), \qu\quad (2.19)$$

where f_w is the wave friction factor, Φ_{τ_0} is the phase lead of the bed shear stress τ_0 over the free stream velocity u_∞. The amplitude of the bed shear stress τ_0 is u_*^2; that is,

$$\overline{\tau}_0 = \frac{\kappa \overline{u}_\infty}{\left| \beta + \varphi\left(\frac{1}{2\beta}\right) + 2\gamma + \ln 2i\beta\zeta_0 \right|} = 1. \quad (2.20)$$

Invoking $\zeta_0 = \omega z_0/(\kappa u_*)$, $\overline{u}_\infty = a\omega/u_*$, and $z_0 = r/30$, where r is the Nikuradse equivalent roughness of the bed, (2.20) reduces to

$$\left| \frac{\beta + \varphi\left(\frac{1}{2\beta}\right) + 2\gamma + \ln 2i\beta\zeta}{\zeta_0} \right| = 30\kappa^2 \frac{a}{r}. \quad (2.21)$$

Using the Newton–Raphson method, ζ_0 can be calculated for each value of a/r and substituted into (2.19) to obtain the friction factor, that is,

$$f_w\left(\frac{a}{r}\right) = 2\frac{\overline{\tau}_0}{\overline{u}_\infty^2} = \frac{2}{\left(30\kappa\zeta_0\frac{a}{r}\right)^2}, \quad (2.22)$$

and then substituted into (2.18b) to obtain Φ_{τ_0}. As $\beta \to 0$, (2.18b) and (2.21) become

$$\overline{\tau}_0 = \overline{\tau}(\zeta \to \zeta_0) = \frac{-\kappa\overline{u}_\infty}{2\gamma + \ln\zeta_0 + i\frac{\pi}{2}}; \quad (2.23a)$$

$$\left| \frac{2\gamma + \ln\zeta_0 + i\frac{\pi}{2}}{\zeta_0} \right| = 30\kappa^2\frac{a}{r}, \quad (2.23b)$$

which are identical to the corresponding formula of the eddy viscosity model (A.6b) and (A.7a).

b. The viscoelastic–diffusion model

To quantitatively evaluate the effects of eddy vertical diffusion, we nondimensionalize the viscoelastic–diffusion model (1.4) by the scalings (2.5) and combine it with the momentum equation (2.6a) and thus have

$$\overline{\tau} = \kappa\zeta\frac{d\overline{u}_d}{d\zeta} + \frac{i\kappa\alpha\zeta}{1 + i\alpha\zeta}\overline{u}_d. \quad (2.24)$$

Different from the viscoelastic model (1.3), the viscoelastic–diffusion model (1.4) does not yield exact analytical solutions that satisfy the governing equations (2.6a) and (2.24) and boundary conditions (2.7a,b). In addition, the boundary conditions (2.7a,b) are not complete at the bed ($z = 0$), so it is not possible to integrate (2.6a) and (2.24) directly starting at the bed. Instead a shooting method has to be implemented [cf. Zou (1995, 1998) for a detailed description of this method] to obtain the numerical solutions to the problem.

Nonetheless, the approximate solutions may be derived analytically by the following manipulations of the governing equations. Substituting (2.24) into (2.6a) leads to

$$\frac{d}{d\zeta}\left(\zeta\frac{d\overline{u}_d}{d\zeta} + \frac{i\alpha\zeta}{1 + i\alpha\zeta}\overline{u}_d \right) = i\overline{u}_d. \quad (2.25)$$

Substituting (2.6a) into (2.25) gives

$$\zeta\frac{d^2\overline{\tau}}{d\zeta^2} + \frac{i\alpha\zeta}{1 + i\alpha\zeta}\frac{d\overline{\tau}}{d\zeta} = i\overline{\tau}. \quad (2.26)$$

Introducing the transformation

$$\overline{\tau} = (1 + i\alpha\zeta)^{-1/2}W \quad (2.27)$$

in (2.26) gives

$$\frac{d^2W}{d\zeta^2} + \left(\frac{3}{4}\frac{\alpha^2}{(1 + i\alpha\zeta)^2} - \frac{i}{\zeta} \right)W = 0. \quad (2.28)$$

For $\zeta \ll 1$, $(3/4)\,[\alpha^2/(1 + i\alpha\zeta)^2] \ll i/\zeta$; therefore, (2.28) is well approximated by

$$\frac{d^2W}{d\zeta^2} - \frac{i}{\zeta}W = 0, \quad (2.29)$$

which is the same as the governing equation of shear stress for the eddy viscosity model; therefore,

$$W = C_1\overline{\tau}_e, \quad (2.30a)$$

where C_1 is a constant coefficient,

$$\overline{\tau}_e = \kappa\overline{u}_\infty\sqrt{i\zeta}\frac{\text{ker}_1 2\sqrt{\zeta} + i\,\text{kei}_1 2\sqrt{\zeta}}{\text{ker} 2\sqrt{\zeta_0} + i\,\text{kei} 2\sqrt{\zeta_0}} \quad (2.30b)$$

is the shear stress solution of the eddy viscosity model (cf. appendix A), ker, kei, ker_1, and kei_1 are the zeroth and first-order Kelvin functions. Substituting (2.30) into (2.27) yields

$$\overline{\tau} = C_1(1 + i\alpha\zeta)^{-1/2}\overline{\tau}_e. \quad (2.31)$$

Substituting (2.31) into (2.6a) gives

$$\overline{u}_d = C_1\left[\overline{u}_{ed}(1 + i\alpha\zeta)^{-1/2} - \frac{\alpha}{2\kappa}\overline{\tau}_e(1 + i\alpha\zeta)^{-3/2} \right], \quad (2.32a)$$

where

$$\overline{u}_{ed} = -\overline{u}_\infty\frac{\text{ker} 2\sqrt{\zeta} + i\,\text{kei} 2\sqrt{\zeta}}{\text{ker} 2\sqrt{\zeta_0} + i\,\text{kei} 2\sqrt{\zeta_0}} \quad (2.32b)$$

is the perturbation velocity solution of the eddy viscosity model (cf. appendix A). Substituting (2.32b) and (2.30b) into (2.32a), we obtain

$$\overline{u}_d = -C_1\overline{u}_\infty\left[\frac{\text{ker} 2\sqrt{\zeta} + i\,\text{kei} 2\sqrt{\zeta}}{\text{ker} 2\sqrt{\zeta_0} + i\,\text{kei} 2\sqrt{\zeta_0}}(1 + i\alpha\zeta)^{-1/2} \right.$$

$$+ \frac{\alpha}{2}\sqrt{i\zeta}\frac{\text{ker}_1 2\sqrt{\zeta} + i\,\text{kei}_1 2\sqrt{\zeta}}{\text{ker} 2\sqrt{\zeta_0} + i\,\text{kei} 2\sqrt{\zeta_0}}$$

$$\left. \times (1 + i\alpha\zeta)^{-3/2} \right]. \quad (2.33)$$

The constant coefficient C_1 is determined by the no-slip boundary condition at the bed (2.7a); that is, $\overline{u}_d = -\overline{u}_\infty$ as $\zeta \to \zeta_0$ so that the velocity solution (2.33) becomes

$$\overline{u} = \overline{u}_\infty + \overline{u}_d = \overline{u}_\infty \left[1 - \frac{F_1(\alpha, \zeta)}{F_1(\alpha, \zeta_0)} \right], \quad (2.34a)$$

where

$$F_1(\alpha, \zeta) = (1 + i\alpha\zeta)^{-1/2} \left[\frac{\text{ker}2\sqrt{\zeta} + i\ \text{kei}2\sqrt{\zeta}}{\text{ker}2\sqrt{\zeta_0} + i\ \text{kei}2\sqrt{\zeta_0}} + \frac{\alpha}{2}\sqrt{i\zeta}\ \frac{\text{ker}_1 2\sqrt{\zeta} + i\ \text{kei}_1 2\sqrt{\zeta}}{\text{ker}2\sqrt{\zeta_0} + i\ \text{kei}2\sqrt{\zeta_0}}(1 + i\alpha\zeta)^{-1} \right] \quad (2.34b)$$

and the shear stress solution (2.31) becomes

$$\overline{\tau} = \kappa\overline{u}_\infty [F_1(\alpha, \zeta_0)]^{-1}(1 + i\alpha\zeta)^{-1/2}$$
$$\times \sqrt{i\zeta}\ \frac{\text{ker}_1 2\sqrt{\zeta} + i\ \text{kei}_1 2\sqrt{\zeta}}{\text{ker}2\sqrt{\zeta_0} + i\ \text{kei}2\sqrt{\zeta_0}}. \quad (2.35)$$

Similar to the velocity and shear stress solutions of viscoelastic model, (2.14) and (2.15), those of viscoelastic–diffusion model, (2.34) and (2.35), reduce to those of the eddy viscosity model, (2.30b) and (2.32b), as $\alpha \to 0$.

Near the surface ($\zeta \to \zeta_0$), $\overline{\tau}$ approaches its asymptotic value of

$$\overline{\tau}_0 = \overline{\tau}(\zeta \to \zeta_0) = \frac{-\kappa\overline{u}_\infty}{2\gamma - \frac{1}{2}\alpha + \ln\zeta_0 + i\frac{\pi}{2}}, \quad (2.36)$$

which is the bed shear stress. The bed shear stress is related to the orbital velocity by

$$\overline{\tau}_0 = \frac{1}{2} f_w |\overline{u}_\infty| \overline{u}_\infty \exp(i\Phi_{\tau_0}), \quad (2.37)$$

where f_w is the wave friction factor and Φ_{τ_0} is the phase lead of the bed shear stress over the free stream velocity u_∞.

The amplitude of the bed shear stress τ_0 is u_*^2; that is,

$$\overline{\tau}_0 = \kappa\overline{u}_\infty \left/ \left| 2\gamma - \frac{\alpha}{2} + \ln\zeta_0 + i\frac{\pi}{2} \right| \right. = 1. \quad (2.38)$$

Invoking $\zeta_0 = \omega z_0/(\kappa u_*)$, $\overline{u}_\infty = a\omega/u_*$ and $z_0 = r/30$, where r is the Nikuradse equivalent roughness of the bed, (2.38) reduces to

$$\left| \frac{2\gamma - \frac{\alpha}{2} + \ln\zeta_0 + i\frac{\pi}{2}}{\zeta_0} \right| = 30\kappa^2 \frac{a}{r}, \quad (2.39)$$

which is identical to the corresponding formula (2.23b) of the eddy viscosity model as $\alpha \to 0$. From (2.39), ζ_0 is calculated for a given value of a/r and substituted into (2.22) and (2.36) to obtain f_w and Φ_{τ_0}. As demonstrated in the next section, solutions (2.34) and (2.35) compare well with the numerical results using the shooting method.

3. Comparison with experiment results

We now compare the present analytical solutions, (2.34) and (2.35), of the viscoelastic–diffusion model, (2.14) and (2.15), of the viscoelastic model as well as those of the eddy viscosity model, (A3) and (A4), with measurements of the oscillatory boundary layer over rough and smooth beds. The former is more relevant to that in the natural environment. According to Jensen et al.'s (1989) measurement, $\alpha = \kappa^2 q^2/\langle u'w' \rangle \approx 2$, so we will first use this value to evaluate the model in the comparisons, then carry out a sensitivity study of the viscoelastic–diffusion model relative to the choice of α.

As demonstrated in Figs. 1a and 1b, in comparison with the eddy viscosity model, the viscoelastic–diffusion model provides improved overall predictions for
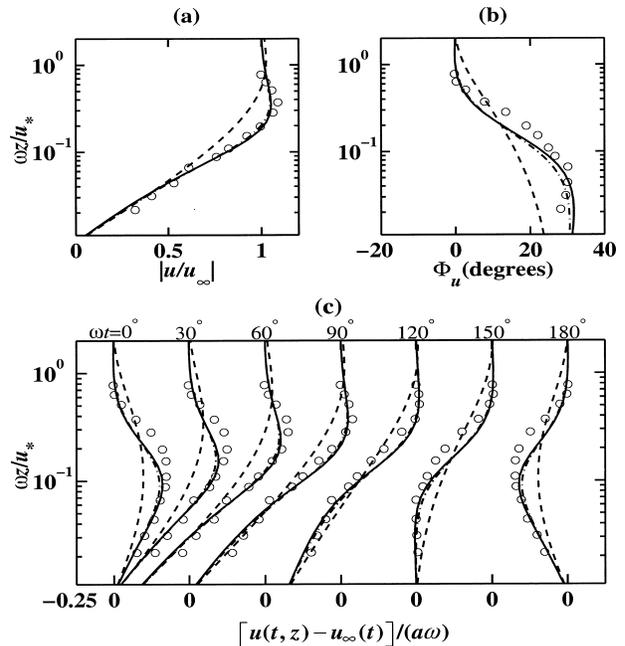

FIG. 1. The predicted and measured (a) magnitude and (b) phase of the dimensionless complex amplitude of velocity, u/u_∞, for the wave boundary layer over a rough bed. (c) Evolution of dimensionless velocity defect, $[u(t, z) - u_\infty(t)]/a\omega$ over one-half wave cycle for a free-stream velocity of $u_\infty = a\omega \sin\omega t$: analytical solution (2.34) (solid lines) and numerical solution (dashed-dot lines) of viscoelastic–diffusion model; the eddy viscosity model solution (2.32b) (dashed lines); Jonsson and Carlsen's (1976) test 2 (circles).
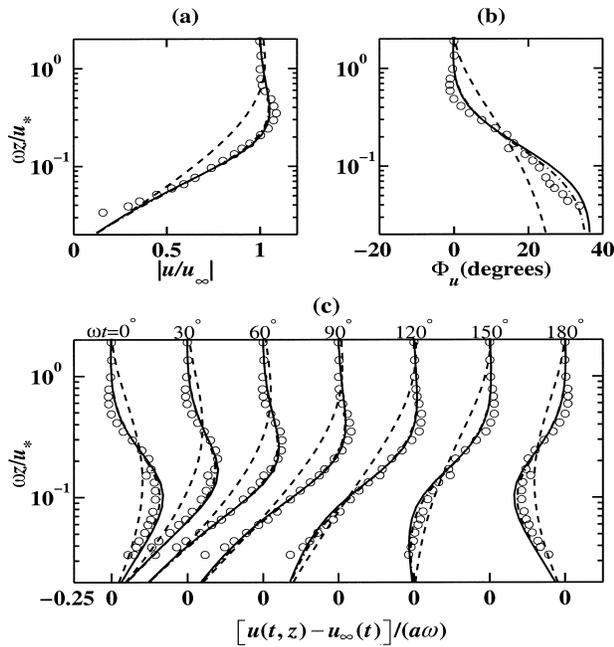
FIG. 2. The predicted and measured (a) magnitude and (b) phase of the dimensionless complex amplitude of velocity, u/u_∞, for the wave boundary layer over a rough bed. (c) Evolution of dimensionless velocity defect, $[u(t, z) - u_\infty(t)]/a\omega$ over one-half wave cycle for a free-stream velocity of $u_\infty = a\omega \sin\omega t$: analytical solution (2.34) (solid lines) and numerical solution (dashed-dot lines) of viscoelastic–diffusion model; the eddy viscosity model solution (2.32b) (dashed lines); Van Doorn (1982) observations (circles).
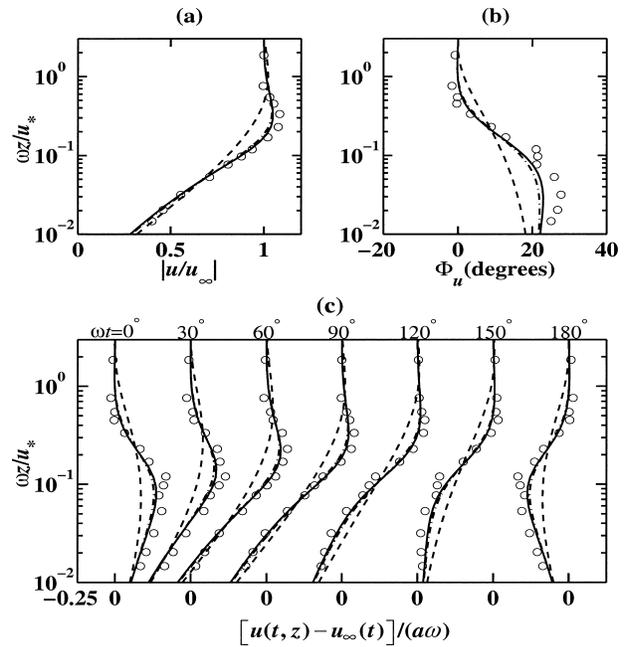
FIG. 3. The predicted and measured (a) magnitude and (b) phase of the dimensionless complex amplitude of velocity, u/u_∞, for the wave boundary layer over a rough bed. (c) Evolution of dimensionless velocity defect, $[u(t, z) - u_\infty(t)]/a\omega$ over one-half wave cycle for a free-stream velocity of $u_\infty = a\omega \sin\omega t$: analytical solution (2.34) (solid lines) and numerical solution (dashed-dot lines) of viscoelastic–diffusion model; the eddy viscosity model solution (2.32b) (dashed lines); Sleath (1987) observations (circles).

the velocity profiles observed by Jonsson and Carlsen (1976). The two models give identical predictions of $|u/u_\infty|$ in the near-bed region, while diverging in the outer region of the boundary layer. Both magnitude and location of the velocity overshoot are well captured by the present model, but poorly by the eddy viscosity model. The two models are also distinct from each other in predicting the observed phase variation of velocity through the wave boundary layer. The improvement represented by the present model is due to the incorporation of turbulent relaxation and diffusion. Also evident from Fig. 1 is the agreement of the analytical solutions (solid lines) with the numerical results (dashed-dot lines) obtained using a shooting method. As shown next, similar conclusions may be drawn from the comparisons between the present model and other observations with different relative roughness lengths.

Given a free stream velocity of $u_\infty = a\omega \sin\omega t$, Fig. 1c shows the temporal evolution of predicted and observed velocity defect profiles, $\overline{u}_d = (u - u_\infty)/u_\infty$, over a half oscillatory cycle. After the flow reversal ($\omega t \approx 0°$), a velocity overshoot is generated near the bed, diffuses away from the bed with time, and intensifies with time until the flow reaches maximum amplitude at midcycle ($\omega t \approx 90°$). During the following decelerating stage, the velocity overshoot continues moving upward but declines in magnitude, and a new velocity overshoot

is generated close to the bed in the opposite direction. Near the midcycle, both the present model and the eddy viscosity model predictions agree with the measurements fairly well in the near-bed region. Farther away from the bed, the two models start to deviate from each other, and the present model is in better agreement with the observations in the velocity overshoot region.

During the period of flow reversal ($\omega t \approx 0°$ and $\omega t \approx 180°$), velocity overshoot comes into existence in both upper and lower parts of the boundary layer, the eddy viscosity model fails to capture the vertical variation of velocity throughout the layer, while the present model remains reasonable agreement with the observations. At this stage of the wave period, turbulence is generated and diffuses away from the bed, therefore has not reached an equilibrium with the mean flow. The associate strong turbulent relaxation and diffusion prohibit it from being adequately described by the eddy viscosity model. After flow maximum, turbulence is well developed and in a close analogy with its counterpart of steady flow, the eddy viscosity model becomes more suitable to characterize its dynamics.

There exists a wide range of relative roughness in both natural wave boundary layers and laboratory experiments. It is therefore useful to examine whether the present model is applicable for turbulent flows with a variety of relative roughness. We carried out similar
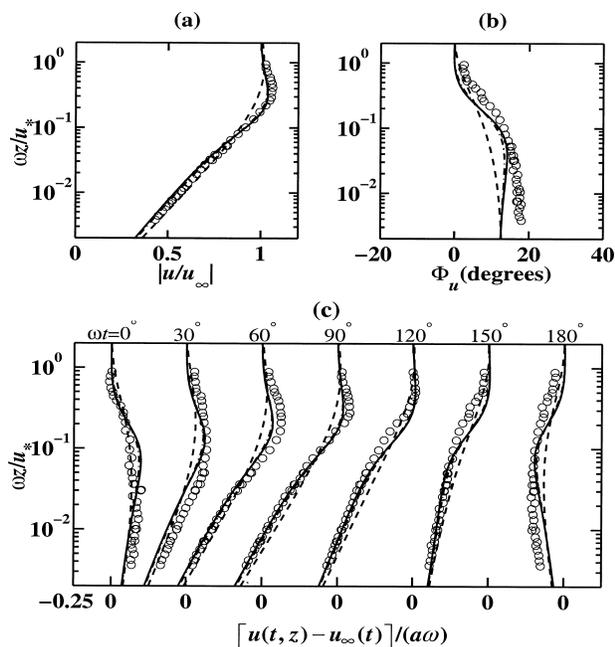
FIG. 4. The predicted and measured (a) magnitude and (b) phase of the dimensionless complex amplitude of velocity, u/u_∞, for the wave boundary layer over a rough bed. (c) Evolution of dimensionless velocity defect, $[u(t, z) - u_\infty(t)]/a\omega$ over one half wave cycle for a free stream velocity of $u_\infty = a\omega \sin\omega t$: analytical solution (2.34) (solid lines) and numerical solution (dashed-dot lines) of viscoelastic–diffusion model; the eddy viscosity model solution (2.32b) (dashed lines); Jensen et al. (1989) test 13 (circles).
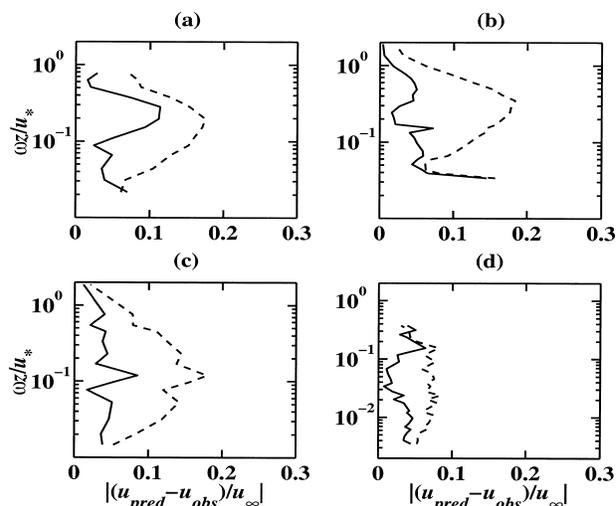

FIG. 5. The discrepancy between the predicted and observed dimensionless complex amplitude of velocity, $|(u_{pred} - u_{obs})/u_\infty|$ for (a) Jonsson and Carlsen's (1976) test 2, (b) Van Doorn (1982), (c) Sleath (1987), and (d) Jensen et al. (1989) test 13: analytical solution (2.34) (solid lines) of viscoelastic–diffusion model; the eddy viscosity model solution (2.32b) (dashed lines).

comparisons with the measurements by Van Doorn (1982), Sleath (1987), and Jensen et al. (1989), and the results are displayed in Figs. 2, 3, and 4, respectively. Table 1 lists wave period T, the semiexcursion amplitude of orbital velocity a, the Nikuradse equivalent roughness length r, and the relative roughness length r/a for these experiments.

From these figures, one may draw similar conclusions to those in the preceding paragraphs from Fig. 1. To further quantify the performance of the viscoelastic–diffusion model relative to the eddy viscosity model in predicting these observations, Fig. 5 illustrates how the discrepancy between two models and observations varies across the boundary layer, and Table 2 lists their averaged values over the boundary layer thickness. Together with the intercomparisons among Figs. 1–4, they suggest the following: 1) the velocity overshoot decreases as the bed roughness becomes smaller; 2) in the

rough bed case, a more rapid deduction of the mean velocity toward the bed is observed due to the enhanced momentum exchange by the increased bed roughness; 3) the deviation of the present model from the eddy viscosity model is dependent on the relative roughness and it is smaller in smooth bed case than in rough bed case; and 4) the discrepancy given by the present model is about one half or one quarter of that by the eddy viscosity model (cf. Fig. 5, Table 2).

Nielsen (1985) was intrigued by the behavior of the nondimensional velocity defect $Du = 1 - u/u_\infty$. He noted that the identity relationship, $\log|Du| \equiv \arg(Du)$, which is valid for laminar flow, also holds with great accuracy for most turbulent flows with reasonable relative roughness. He also pointed out that neither the eddy viscosity models nor the numerical mixing length models are able to reproduce this behavior. In case of a rough bed, as demonstrated by Fig. 6a, the observed profiles of $-\log|Du|$ and $-\arg(Du)$ satisfy this relationship, while in case a smooth bed, as demonstrated by Fig. 6b, they diverge from each other significantly.

TABLE 1. The key parameters for the laboratory measurements of WBL.

Parameters	T (s)	a (m)	r (m)	r / a
Jonsson and Carlsen (1976)	7.2	1.79	0.063	0.0352
Van Doorm (1982)	2	0.33	0.021	0.0636
Sleath (1987)	4.58	0.45	0.003 26	0.0072
Jensen et al. (1989)	9.7	3.1	0.000 84	0.000 27

TABLE 2. The average discrepancy between predicted and observed velocity over the boundary layer thickness.

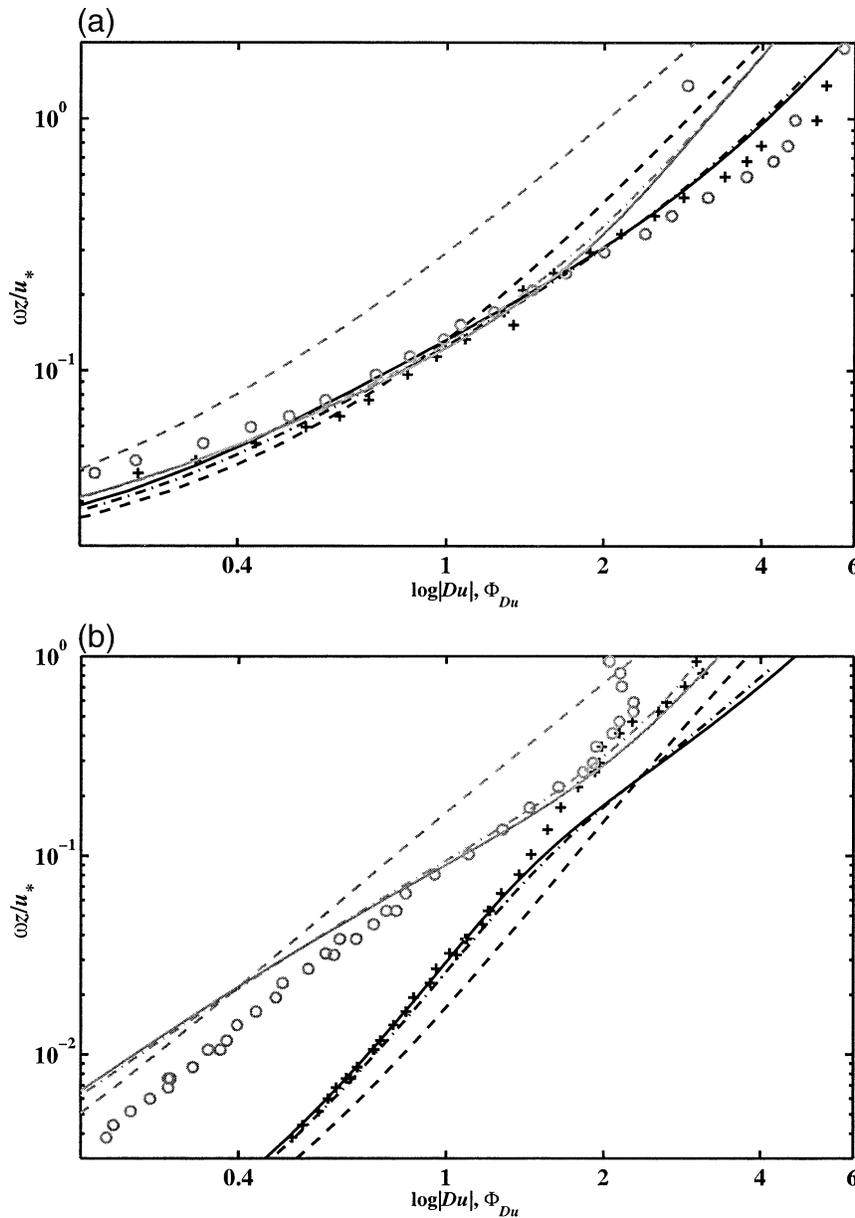|		$[\int |u_{pred}(z) - u_{obs}(z)|^2/|u_\infty|^2 \, dz]^{1/2}$	
Experiments	r/a	Viscoelastic–diffusion	Eddy viscosity
Jonsson and Carlsen (1976)	0.035	0.062	0.12
Van Doorn (1982)	0.064	0.028	0.094
Sleath (1987)	0.0072	0.027	0.073
Jensen et al. (1989)	0.000 27	0.041	0.056

FIG. 6. (a) The predicted and measured dimensionless complex amplitude of velocity defect $Du = 1 - u/u_\infty$ for rough bed: $-\ln|Du|$ (dark) and $-\arg(Du)$ (gray): analytical solution (2.34) (solid lines) and numerical solution (dashed-dot lines) of viscoelastic–diffusion model (1.3); the eddy viscosity model solution (2.32b) (dashed lines), Van Doorn (1982) Test M10 RAL (pluses and circles). (b) Jensen et al. (1989) test 13 (pluses and circles).

This behavior is well captured by the present model but not by the eddy viscosity model.

Figure 7a illustrates the temporal evolution of the predicted and observed shear stress profile over a half oscillatory cycle. During the accelerating stage, turbulence is generated near the bed, diffuses away from the bed with time until midcycle when it starts to distribute uniformly across the layer. During the decelerating stage, the adverse pressure gradient comes into play, it enhances the shear instability according to the inflection point criterion, which is in analogy to the separating flow in the steady turbulent flow. As a result, turbulence is intensified at the bed, moves upward, and decays until the flow starts to reverse and new eddies are created near the bed (cf. Jensen et al. 1989). The elevation of zero shear stress marks the division between the new and old turbulence. According to the observations, it moves from close to the bed to the top of the boundary layer within a half cycle. The other important feature exhibited in this figure is the shear stress overshoot mov-
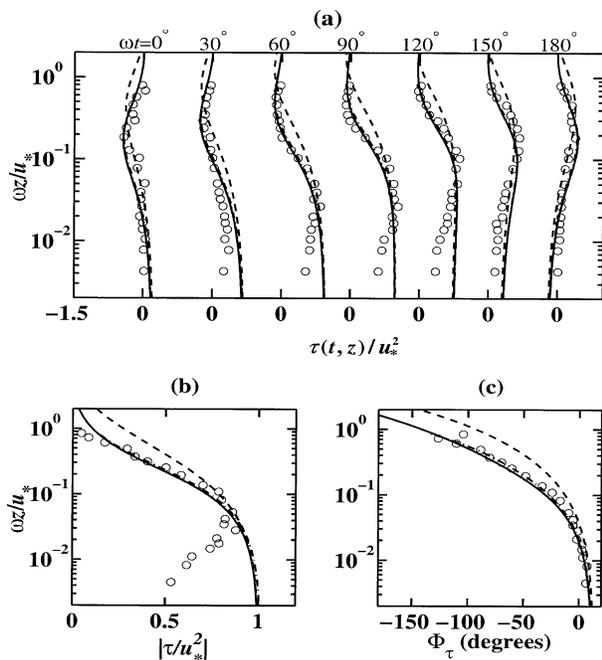
FIG. 7. (a) Evolution of dimensionless shear stress profile, $\tau(t, z)/u_*^2$, over one-half wave cycle. The predicted and measured (b) magnitude and (c) phase of the complex amplitude of shear stress τ/u_*^2: analytical solution (2.35) (solid lines) and numerical solution (dashed-dot lines) of viscoelastic–diffusion model; the eddy viscosity model solution (2.30b) (dashed lines), Jensen et al. (1989) test 13 (circles).
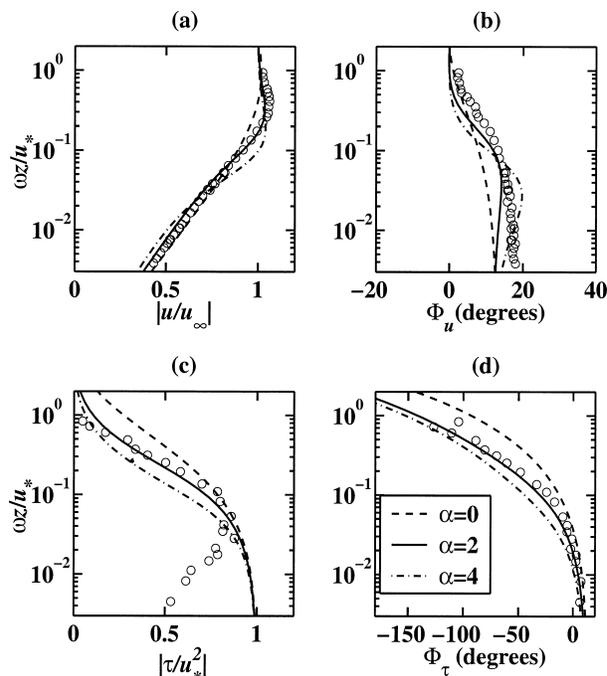
FIG. 8. Comparison of the observed (a), (c) magnitude and (b), (d) phase of velocity and shear stress by Jensen et al. (1989) with the predictions by the analytical solutions (2.34) and (2.35) of viscoelastic–diffusion model using three different values of α; i.e., $\alpha = 0$ (the eddy viscosity model; dashed lines), $\alpha = 2$ (the present model; solid lines), and $\alpha = 4$ (dashed-dot lines).

ing upward with time. This feature is in connection with the similar upward motion of the velocity overshoot shown by Fig. 4c. The eddy viscosity model is unable to track either of the observations for these events, whereas the present model does an excellent job in predicting their elevations as well as the overshoot magnitude of shear stress.

The difference between these two models in predicting the observed shear stress profile is further elucidated in Figs. 7b and 7c where only the magnitude and phase of its complex amplitude are exhibited. The two models are identical to each other in the near-bed region while separate from each other farther up in the water column, where the present model gives improved prediction of the decreasing magnitude and phase of shear stress with the height above the bed. Nonetheless, it is noticeable in both Figs. 7a and 7b that neither model predicts the shear stress magnitude well right next to the bed.

Both Sleath (1987) and Jensen et al. (1989) noticed that due to the reflection of the laser beam off the bed, the laser-Doppler anemometer (LDA) tends to underestimate the shear stress in this region. Alternatively, the bed shear stress was estimated from the logarithmic fit of the near-bed velocity profile and through the momentum integration method (cf. Jensen 1989). The former was used to derive the observed friction factor f_w (denoted as circles) in Figs. 10 and 11, while the later is listed as u_*^2 in Table 1 of Jensen et al. (1989) and

used as the scaling for nondimensionalizing the shear stress. They are consistent with each other and with the prediction by viscoelastic–diffusion model with $\alpha = 2$ as shown in Fig. 10. They are, however, almost twice as much as that given by LDA at the measuring point closest to the bed (cf. Fig. 7b).

As pointed out in the introduction, the phase lead of shear stress Φ_τ relative to the free stream velocity is an important quantity in studies of wave dissipation and sediment transport and suspension in the ocean bottom boundary layers. As shown in Figs. 7b and 7c, the present model (solid lines) predicts Φ_τ remarkably well across the whole layer, whereas the eddy viscosity model (dashed lines) underestimates Φ_τ and the discrepancy increases with the height above the bed. This deviation is mainly attributed to the turbulent relaxation effect neglected by the eddy viscosity model. From (1.3), we have the phase of the effective eddy viscosity in the form of $\Phi_\nu = -\arctan(\alpha z/l)$; accordingly, Φ_ν of viscoelastic models decreases from zero at the bed to about $-90°$ at the top of wave boundary layer, whereas Φ_ν of the eddy viscosity model remains zero across the layer.

According to the viscoelastic model (1.3), $\beta = \sqrt{\alpha}$ is a weight coefficient of eddy relaxation since, as $\beta \to 0$, (1.3) reduces to the eddy viscosity model. It is worthwhile examining how α affects the results. Therefore, we applied $\alpha = 0$ (the eddy viscosity model, denoted by dashed lines), $\alpha = 2$ (the present model, solid lines),
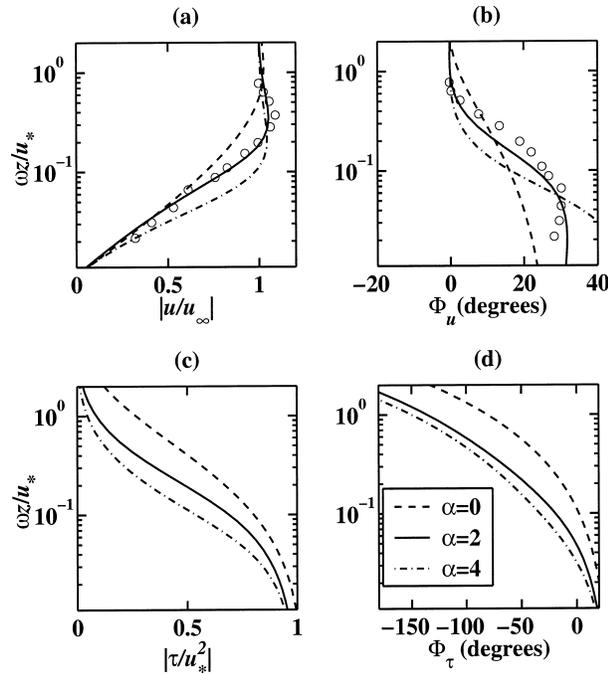
FIG. 9. Comparison of the observed (a), (c) magnitude and (b), (d) phase of velocity and shear stress profiles by Jonsson and Carlsen (1976) with the predictions by the analytical solutions (2.34) and (2.35) of viscoelastic–diffusion model using three different values of α; i.e., $\alpha = 0$ (the eddy viscosity model, dashed lines), $\alpha = 2$ (the present model, solid lines), and $\alpha = 4$ (dashed-dot lines).

FIG. 10. Friction factor (a) and phase lead (b) of the bed shear stress over the free stream velocity as a function of a/r. The predictions by the viscoelastic–diffusion model using three different values of α [cf. Eqs. (2.39), (2.22), and (2.36)]; i.e., $\alpha = 0$ (the eddy viscosity model; dashed lines), $\alpha = 2$ (the present model; solid lines), and $\alpha = 4$ (dashed-dot lines) and by the k–ε turbulent closure model (denoted by diamonds; cf. Justesen 1988). The observed results by Kamphuis (1975) (denoted by X), Jonsson and Carlsen (1976) (denoted by +), Sleath (1987) (denoted by *), and Jensen et al. (1989) (denoted by ○).

and $\alpha = 4$ (dashed-dot lines) to the viscoelastic–diffusion solutions (2.34) and (2.35). The predicted velocity and shear stress profiles are exhibited in Figs. 8 and 9 together with the measurements by Jensen et al. (1989) and Jonsson and Carlsen (1976) respectively. Both figures suggest that, while $\alpha = 0$ and $\alpha = 2$ yield the diverging results that have been thoroughly discussed in the preceding paragraphs, $\alpha = 2$ and $\alpha = 4$ predict identical magnitudes of velocity and shear stress overshoot, but only the former manages to locate the velocity and shear stress overshoot correctly.

The friction factor f_w and phase lead of the bed shear stress over free stream velocity, Φ_{τ_0}, are both important quantities to evaluate in any theoretical model of this problem. Figure 10 shows the predictions by (2.39), (2.22), and (2.36) for the viscoelastic–diffusion model with $\alpha = 0$, 2, and 4 together with the measurements of f_w and Φ_{τ_0} for $10^4 \geq a/r \geq 10^1$ by Kamphuis (1975), Jonsson and Carlsen (1976), Sleath (1987), and Jensen et al. (1989). The predicted f_w and Φ_{τ_0} decrease with increasing α and the deviations reduce considerably for small relative roughness r/a. The viscoelastic–diffusion model with $\alpha = 2$ (denoted by solid line) provides the optimal prediction of the observed f_w at $a/r > 10^2$ while underpredicting it at a larger roughness $a/r < 10^2$. This result is consistent with the fact that $\alpha = 2$ gives the optimal prediction of the observed
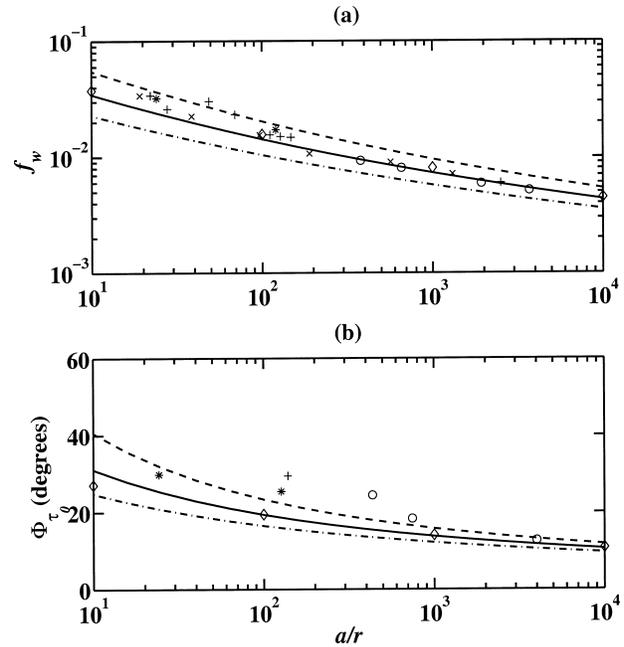
velocity and shear stress profiles (cf. Figs. 8 and 9). Also evident from Figs. 10a and 10b is the close approximation between the predictions by the viscoelastic–diffusion model with $\alpha = 2$ and those by the more sophisticated k–ε turbulent closure model (denoted by diamonds: cf. Justesen 1988). The deviation between theory and observation at $a/r < 10^2$ is probably due to the significant form drag associated with the large roughness element in this parameter region, which is not included in the theory or models.

The same comparison was conducted in Fig. 11 for the predictions by the viscoelastic model solutions (2.21), (2.22), and (2.18b) with $\alpha = 0$, 2, and 4. Similar to the viscoelastic–diffusion model, the predicted f_w and Φ_{τ_0} decrease with increasing α and the deviations decrease for small relative roughness r/a. The intercomparison between Figs. 10 and 11 and Table 3 indicates that the predicted f_w and Φ_{τ_0} by the viscoelastic model using $\alpha = 4$ is approximately the same as those by the viscoelastic–diffusion model using $\alpha = 2$ and by the k–ε turbulent closure model.

The sensitivity study of model parameter α is carried out further in Fig. 12. According to Fig. 12a, the depth-averaged velocity discrepancy between the viscoelastic–diffusion model and observation attains a minimum val-
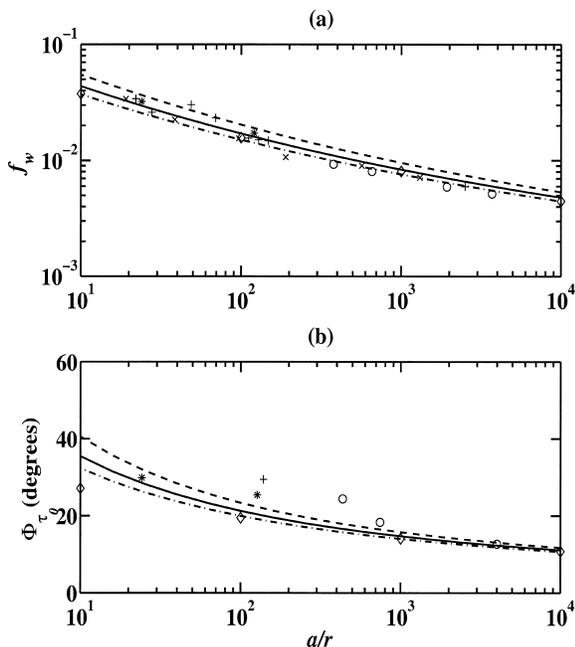
FIG. 11. Friction factor (a) and phase lead (b) of the bed shear stress over the free stream velocity as a function of a/r. The predictions by the viscoelastic model using three different values of α [cf. Eqs. (2.21), (2.22), (2.18b)]; i.e., $\alpha = 0$ (the eddy viscosity model; dashed lines), $\alpha = 2$ (the present model; solid lines), and $\alpha = 4$ (dashed-dot lines) and by the k–ε turbulent closure model (denoted by diamonds; cf. Justesen 1988). The observed results by Kamphuis (1975) (denoted by X), Jonsson and Carlsen (1976) (denoted by +), Sleath (1987) (denoted by *), and Jensen et al. (1989) (denoted by ○).

ue of 0.05, 0.027, 0.027, and 0.028 at $\alpha = 1.5$, 2.1, 2.2, and 1.2 for Jonsson and Carlsen (1976), Van Doorn (1982), Sleath (1987), and Jensen et al. (1989), respectively. As listed in Table 2, the discrepancy goes up to 0.12, 0.09, 0.07, and 0.06 at $\alpha = 0$ for the eddy viscosity model.

To study the effects of turbulent diffusion separately from those of turbulent relaxation, we compare the velocity and shear stress solutions according to the viscoelastic–diffusion model (1.4), the viscoelastic model (1.1), the eddy viscosity model, as well as the viscoelastic model with exponentially decaying mixing length (B.1). Figures 13 and 14 illustrate the comparisons for smooth and rough bed respectively. As dem-

onstrated in these figures, in contrast to the eddy viscosity model, the viscoelastic and viscoelatic–diffusion models result in identical phase shifts for shear stress. Both of them are able to resolve the feature of overshooting velocity and shear stress. However, the viscoelastic model overestimates their heights and magnitudes. This deficiency is due to the turbulent diffusion neglected in the model, which tends to reduce the magnitudes of velocity and shear stress at the top of boundary layer. Unlike turbulent diffusion, turbulent relaxation is more relevant to the phase variations of velocity and shear stress in the vertical direction.

4. Conclusions and discussions

In this work, by adding viscoelastic and diffusion terms to the conventional eddy viscosity model, we have constructed a viscoelastic–diffusion model to study the turbulent relaxation and diffusion effects in oscillatory boundary layers [cf. Eq. (1.4)]. The resulting analytical solutions are found to be in better agreement with observations than the previous solutions using time-invariant eddy viscosity and time-variant eddy viscosity models such as that by Madsen and Wikramanayake (1991, cf. their Fig. 26). Our analysis shows that the turbulent relaxation plays a key role in the phase variations of velocity and shear stress in the vertical direction, whereas the turbulent diffusion is mainly responsible for reducing the magnitude of these variables at the top of the boundary layer.

The present study yields a complex eddy viscosity instead of the real one assumed by the eddy viscosity models. Furthermore, unlike most eddy viscosity models (Kajiura 1968; Johns 1969; Grant 1977; Smith 1977; Brevik 1981; Myrhaug 1982; Lavelle and Mofjeld 1983; Trowbridge and Madsen 1984; Davies 1986; Madsen and Wikramanayake 1991), the viscoelastic diffusion model (1.4) does not involve any discontinuity in eddy viscosity or its gradient and requires no pre-assumption of matching height between adjacent layers. The merit of this modification is demonstrated by the better agreement between predicted and observed phase variations and the magnitude of the velocity and shear stress profiles.

The viscoelastic–diffusion model provides a good prediction of the velocity profile in both inner and outer regions of the boundary layer at any phase of wave

TABLE 3. The friction factor f_w calculated by the eddy viscosity, viscoelastic, viscoelastic–diffusion, and k–ϵ models.

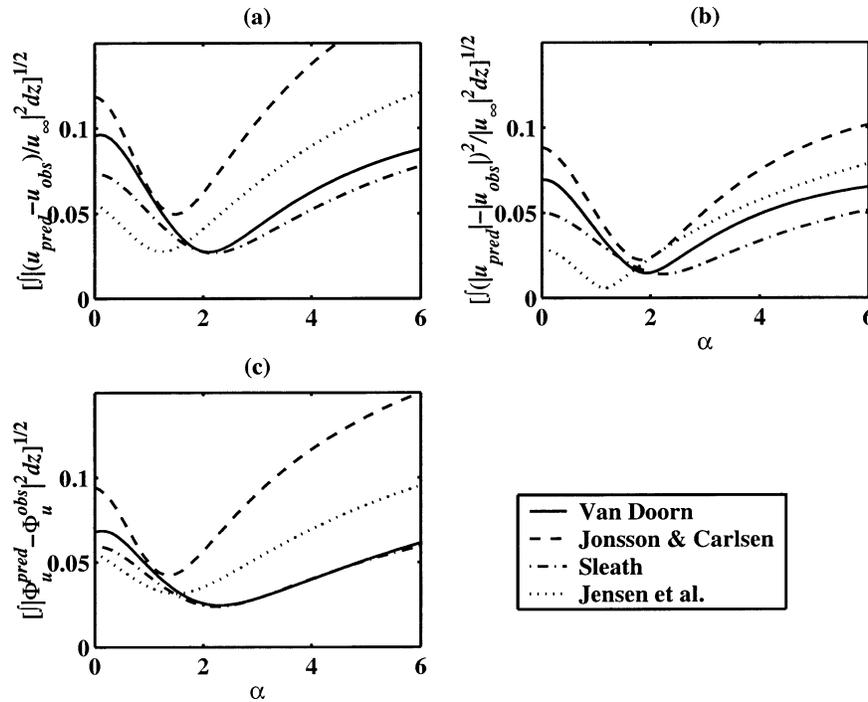| | | f_w | | | | |
| | | Viscoelastic | | Viscoelastic–diffusion | | |
a/r	Eddy viscosity	$\alpha = 2$	$\alpha = 4$	$\alpha = 2$	$\alpha = 4$	k–ϵ model
10^1	0.055	0.044	0.037	0.035	0.023	0.038
10^2	0.020	0.017	0.015	0.014	0.010	0.016
10^3	0.0096	0.0084	0.0076	0.0073	0.0057	0.0081
10^4	0.0053	0.0048	0.0045	0.0043	0.0035	0.0045

FIG. 12. The depth averaged discrepancy between the predicted and observed (a) dimensionless complex amplitude of velocity $[\int |(u_{\mathrm{pred}} - u_{\mathrm{obs}})/u_\infty|^2 \, dz]^{1/2}$, (b) its amplitude $[\int (|u_{\mathrm{pred}}| - |u_{\mathrm{obs}}|)^2 / |u_\infty|^2 \, dz]^{1/2}$, and (c) phase $[\int |\Phi_u^{\mathrm{pred}} - \Phi_u^{\mathrm{obs}}|^2 \, dz]^{1/2}$: Jonsson and Carlsen's (1976) test 2 (dashed lines); Van Doorn (1982) (solid lines); Sleath (1987) (dashed-dot lines); and Jensen et al. (1989) test 13 (dotted lines).

cycle. Thus, the present velocity solution serves as a better candidate than that of the eddy viscosity model for estimating the roughness length and friction velocity from velocity profile measurements in the laboratory and field (cf. Zou and Hay 2002, manuscript submitted to *J. Phys. Oceanogr.*). Furthermore, the comparisons between the predicted and observed velocity and shear stress profiles, the friction factor f_w and phase lead of the bed shear stress over free stream velocity, Φ_{τ_0}, over a smooth bed and a rough bed suggest that the deviation of the present model and the eddy viscosity model increases with increasing relative roughness. In the presence of a rough bed, for a given free-stream velocity, the friction velocity is greater; so is the boundary layer thickness and eddy length scale $l_e = \kappa z$. It follows that eddies with longer life span dominate the turbulent dynamics, which results in more significant eddy relaxation and diffusion effects.

As observed by Sleath (1987) and Jensen et al. (1989), the turbulence intensity showed a significant variation during an oscillatory cycle. To incorporate this characteristic, Lavelle and Mofjeld (1983), Trowbridge and Madsen (1984), Davies (1986), and Madsen and Wikramanayake (1991) have used time-variant eddy viscosity models in their investigations of this problem. They have found that such modification improved the model comparisons with observed streaming velocity and wave–current interaction at an oblique angle. Nev-

ertheless, these models all assume that the time-dependent part of the eddy viscosity has the same vertical structure as the steady part. As pointed out by some of these authors, this physically unrealistic assumption makes it unlikely that these models correctly resolve the vertical structure of streaming velocity within the wave bottom boundary layers. Therefore, it is worth revisiting this problem with a time-variant viscoelastic–diffusion model.

In summary, turbulent relaxation and diffusion have significant effects on the overshooting of velocity and shear stress, their phase variations across the wave boundary layers, as well as the magnitude and phase of bed shear stress. By including these effects, the present model obtains better agreement with the observations of these properties by previous investigators than the eddy viscosity model. It also provides readily evaluated solutions in a closed form which are applicable to both smooth and rough beds.
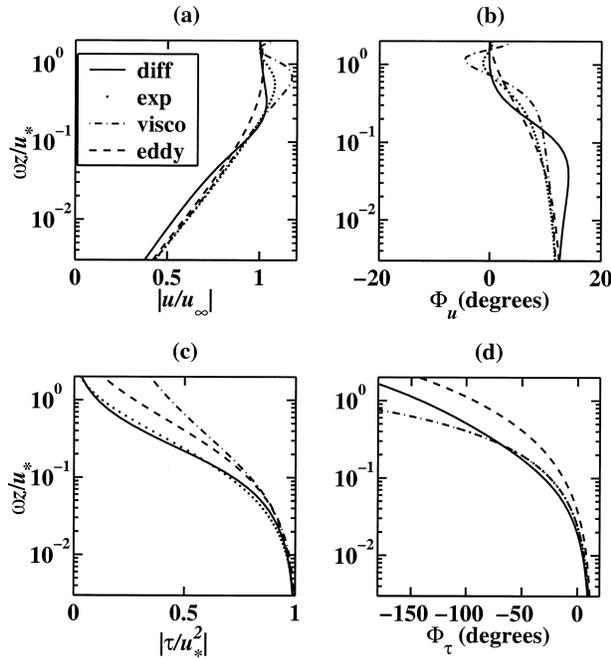
FIG. 13. The predicted and observed (a), (c) magnitude and (b), (d) phase of velocity and shear stress for Jensen et al. (1989) by the viscoelastic–diffusion model [Eqs. (2.34) and (2.35); solid lines]; the eddy viscosity model [Eqs. (2.30b) and (2.32b); dashed lines]; the exponentially decayed viscoelastic model [Eqs. (B.4) and (B.5); dotted lines], and the viscoelastic model [Eqs. (2.14) and (2.15); dashed-dot lines].
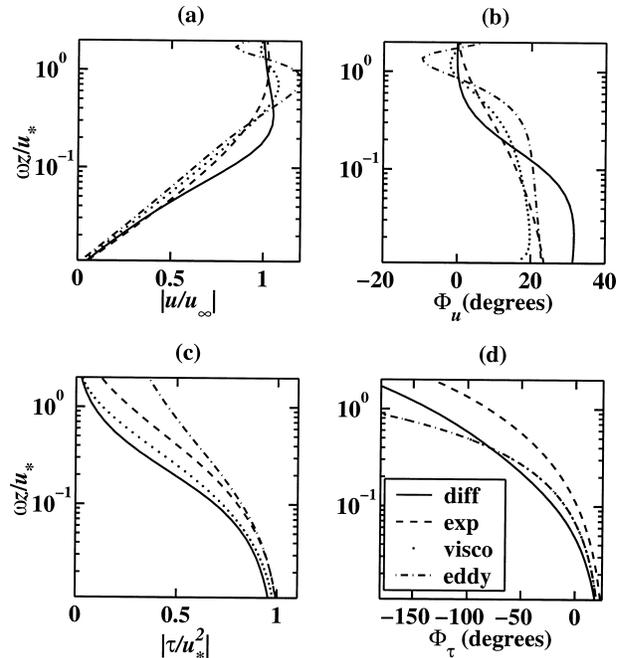
FIG. 14. Comparisons of the predicted and observed (a), (c) magnitude and (b), (d) phase of velocity and shear stress for Jonsson and Carlsen (1976) by the viscoelastic–diffusion model [Eqs. (2.34) and (2.35); solid lines]; the eddy viscosity model [Eqs. (2.30b) and (2.32b); dashed lines]; the exponentially decayed viscoelastic model [Eqs. (B.4) and (B.5); dotted lines], and the viscoelastic model [Eqs. (2.14) and (2.15); dashed-dot lines].

APPENDIX A

Comparison with Previous Eddy-Viscosity Model

To check the consistency of analytical solutions (2.14) and (2.15), we derive the asymptotic behaviors as $\beta \to 0$ and compare them with those of the eddy-viscosity model (cf. Grant 1977). The following relationship is valid for confluent hypergeometric functions (cf. Abramowitz and Stegun 1970, sec. 13.3.3):

$$\lim_{\beta \to 0} \Gamma\left(\frac{1}{2\beta}\right) U\left(\frac{1}{2\beta}, 1, 2i\beta\zeta\right) = 2K_0(2\sqrt{i\zeta}). \quad (A.1)$$

Similarly, we have

$$\lim_{\beta \to 0} \Gamma\left(\frac{1}{2\beta}\right) U\left(1 + \frac{1}{2\beta}, 2, 2i\beta\zeta\right)$$
$$= 2(i\zeta)^{-1/2} K_1(2\sqrt{i\zeta}). \quad (A.2)$$

Substituting (A.1) and (A.2) into (2.14), we have

$$u = u_\infty\left(1 - \frac{\ker 2\sqrt{\zeta} + i \kei 2\sqrt{\zeta}}{\ker 2\sqrt{\zeta_0} + i \kei 2\sqrt{\zeta_0}}\right) \quad (A.3)$$

$$\tau = \kappa u_* u_\infty \sqrt{i\zeta} \frac{\ker_1 2\sqrt{\zeta} + i \kei_1 2\sqrt{\zeta}}{\ker 2\sqrt{\zeta_0} + i \kei 2\sqrt{\zeta_0}}. \quad (A.4)$$

Solutions (A.3) and (A.4) are identical to those by Grant (1977) using the eddy viscosity model. Near the surface ($\zeta \to \zeta_0$), u approaches its asymptotic values of

$$u(\zeta \to \zeta_0) = u_\infty\left\{1 - \frac{1}{2}\frac{2\gamma + \ln\zeta + i\pi/2}{\ker 2\sqrt{\zeta_0} + i \kei 2\sqrt{\zeta_0}}\right\} \quad (A.5a)$$

$$= \frac{-u_\infty}{2\gamma + \ln\zeta_0 + i\pi/2} \ln\frac{\zeta}{\zeta_0}, \quad (A.5b)$$

which is a logarithmic velocity profile, while τ approaches its asymptotic value of

$$\tau_0 = \tau(\zeta \to \zeta_0) = \frac{1}{2}\frac{\kappa u_* u_\infty}{\ker 2\sqrt{\zeta_0} + i \kei 2\sqrt{\zeta_0}} \quad (A.6a)$$

$$= \frac{-\kappa u_* u_\infty}{2\gamma + \ln\zeta_0 + i\pi}, \quad (A.6b)$$

which is the bed shear stress. Following the same procedure as in section 2, we derive the following implicit equation for ζ_0:

$$\frac{|2\gamma + \ln\zeta_0 + i\pi/2|}{\zeta_0} = 30\kappa^2\frac{a}{r} \qquad \text{(A.7a)}$$

$$f_w = \frac{2}{\left(30\kappa\zeta_0\dfrac{a}{r}\right)^2}. \qquad \text{(A.7b)}$$

APPENDIX B

Exponential Decay Viscoelastic Model

As the outer region of wave turbulent layer is approached, the shear stress profile starts to display an exponential decay. Since the turbulent dissipation time is about the same as turbulent relaxation time T_e and in the outer region the eddy-evolving time is about $1/\omega$, the turbulent intensity decays like $\exp(-\omega T_e) = \exp(-\zeta)$ as its origin at the bed. Accordingly, we add an exponential decay coefficient to both the original eddy viscosity ν_0 and the viscoelastic term in (1.3); namely that,

$$\nu = \frac{\nu_0 \exp(-\zeta)}{1 + i\alpha\zeta \exp(-\zeta)}. \qquad \text{(B.1)}$$

Effective eddy viscosity (B.1) is equivalent to (1.3) except at $z \approx l$. Following the same procedure as that in section 3, we derive the governing equation:

$$\frac{\zeta \exp(-\zeta)}{1 + i\alpha\zeta \exp(-\zeta)} \frac{\partial^2\overline{\tau}}{\partial^2\zeta} = i\overline{\tau}, \qquad \text{(B.2)}$$

where $\overline{\tau} = \tau/u_*^2$ is nondimensional shear stress, $\zeta = z/l$ and $\alpha = \kappa^2/a_1$. The shear stress is related to velocity defect by

$$\overline{\tau} = \frac{\zeta \exp(-\zeta)}{1 + i\alpha\zeta \exp(-\zeta)} \frac{\partial\overline{u}_d}{\partial\zeta}, \qquad \text{(B.3)}$$

where $\overline{u}_d = (u - u_\infty)/u_*$ is nondimensional velocity defect.

Equations (B.2) and (B.3) are analytically intractable. A simple WKB analysis shows that their solutions display an exponentially decaying asymptotic behavior at a very large ζ. Eqs. (B.2) and (B.3) become equivalent to (2.6) and (2.4b) when $\zeta \ll 1$. Accordingly, we estimate their solutions by multiplying (2.14) and (2.15) with $\exp(-\zeta/2)$; that is,

$$u = u_\infty\left[1 - \frac{F(\beta, \zeta)}{F(\beta, \zeta_0)}\right]\exp\left(-\frac{\zeta}{2}\right) \qquad \text{(B.4)}$$

$$\tau = -i\kappa u_* u_\infty[F(\beta, \zeta_0)]^{-1}\zeta$$

$$\times \exp(-i\beta\zeta)U\left(1 + \frac{1}{2\beta}, 2, 2i\beta\zeta\right)\exp\left(-\frac{\zeta}{2}\right). \quad \text{(B.5)}$$

The solutions to equation (B.2) and (B.3) are then calculated numerically using the shooting method described in Zou (1995) and Zou (1998). To test the code, we use it to compute the solutions to Eq. (2.6) and boundary conditions (2.7) and then compare the results with analytical solutions (2.14) and (2.15). It was found that the analytical solutions (B.4) and (B.5) are in excellent agreement with the numerical results.

As expected, the predictions are identical to those given by the viscoelastic model at $\zeta < 1$, but the comparisons between theory and experiment are improved remarkably at $\zeta \geq 1$. It is also noticeable that neither phase lead of shear stress Φ_τ nor that of velocity Φ_u is influenced by this modification except that prediction of Φ_u near the bed is improved.

REFERENCES

Abramowitz, M., and I. A. Stegun, Eds., 1970: *Handbook of Mathematical Functions. With Formulas, Graphs and Mathematical Tables.* U.S. National Bureau of Standards, 1046 pp.

Agrawal, Y. C., E. A. Terray, M. A. Donelan, P. A. Hwang, A. J. Williams III, W. M. Drennan, K. K. Kahma, and K. K. Kitaigorodsk, 1992: Enhanced dissipation of kinetic energy beneath surface waves. *Nature,* **359** (6392), 219–220.

Bradshaw, P., D. H. Ferris, and N. P. Atwell, 1967: Calculation of boundary layer development using the turbulent kinetic energy equation. *J. Fluid Mech.,* **30,** 241–258.

Brereton, G. J., and R. R. Mankbadi, 1995: Review of recent advances in the study of unsteady turbulent internal flows. *Appl. Mech. Rev.,* **48** (4), 189–212.

Brevik, I., 1981: Oscillatory rough turbulent boundary layers. *J. Waterw. Port Coastal Ocean Div., ASCE,* **107** (WW3), 175–188.

Davies, A. G., 1977: A mathematical model of sediment in suspension in a uniform reversing tidal flow. *Geophys. J. Roy. Astron. Soc.,* **51,** 503–529.

——, 1986: A model of oscillatory rough turbulent boundary layer flow. *Estuarine Coastal Shelf Sci.,* **23,** 353–374.

Dyer, K. R., 1986: *Coastal and Estuarine Sediment Dynamics.* John Wiley & Sons, 342 pp.

Fredsoe, J., and R. Deigaard, 1992: *Mechanics of Coastal Sediment Transport.* World Scientific, 369 pp.

Gordon, C. M., 1974: Intermittent momentum transport in a geophysical boundary layer. *Nature,* **248,** 392–394.

Grant, W. D., 1977: Bottom friction factor under waves in the presence of a weak current: Its relationship to coastal sediment transport. Sc.D. thesis, Massachusetts Institute of Technology, 275 pp.

——, and O. S. Madsen, 1986: The continental shelf bottom boundary layer. *Annu. Rev. Fluid Mech.,* **18,** 265–305.

Hanjalic, K., 1994: Advanced turbulent closure models. *Int. J. Heat Fluid Flow,* **15,** 178–208.

Hay, A. E., and A. J. Bowen, 1994: Space–time variability of sediment suspension in the nearshore zone. *Proc. Coastal Dynamics '94,* Barcelona, Spain, ASCE, 962–975.

Jensen, B. L., 1989: Experimental investigation of turbulent oscillatory boundary layers. Series paper No. 45, Institute of Hydrodynamics and Hydraulic Engineering, Technical University of Denmark, 157 pp.

——, B. M. Sumer, and J. Fredsoe, 1989: Turbulent oscillatory boundary layers at high Reynolds numbers. *J. Fluid Mech.,* **116,** 265–298.

Johns, B., 1969: On the mass transport induced by oscillatory flow in a turbulent boundary layer. *J. Fluid Mech.,* **43,** 177–185.

Jonsson, I. G., and N. A. Carlsen, 1976: Experimental and theoretical investigations in an oscillatory turbulence boundary layer. *J. Hydraul. Res.,* **14,** 45–60.

Justesen, P., 1988: Turbulent wave boundary layer. Series paper No. 43, Institute of Hydrodynamics and Hydraulic Engineering, Technical University of Denmark, 226 pp.

Kajiura, K., 1968: A model of the bottom boundary layer in water waves. *Bull. Earthquake Res. Inst., Univ. Tokyo,* **46,** 75–123.

Kamphuis, J. W., 1975: Friction factor under oscillatory waves. *J. Waterw. Port Coastal Eng. Div., ASCE,* **101** (WW2), 135–144.

Lavelle, J. W., and H. O. Mofjeld, 1983: Effects of time-varying viscosity on oscillatory turbulent channel flow. *J. Geophys. Res.,* **88** (C12), 7607–7616.

Madsen, O. S., and P. N. Wikramanayake, 1991: Simple model for turbulent wave-current bottom boundary layer flow. Contract Rep. DRP-91-1, U.S. Army Corps of Engineers, Coastal Engineering Research Center, Vicksburg, MS, 150 pp.

McLean, S. R., 1983: Turbulence and sediment transport measurements in a North Sea tidal inlet (The Jade). *North Sea Dynamics,* C. Sundermann and W. Lentz, Eds., Springer-Verlag, 436–452.

Myrhaug, D., 1982: On a theoretical model of rough turbulent wave boundary layers. *Ocean Eng.,* **9,** 547–565.

Nielsen, P., 1985: On the structure of oscillatory boundary layers. *Coastal Eng.,* **9,** 261–276.

——, 1992: *Coastal Bottom Boundary Layers and Sediment Transport.* World Scientific, 324 pp.

Olver, F. W. J., 1974: *Asymptotics and Special Functions.* Academic Press, 572 pp.

Sleath, J. F. A., 1987: Turbulent oscillatory flow over rough beds. *J. Fluid Mech.,* **182,** 369–409.

——, 1990: Seabed boundary layers. *The Sea,* B. LeMehaute and D. M. Hanes, Eds., Ocean Engineering Science, Vol. 9, Wiley and Sons 239–292.

Smith, J. D., 1977: Modeling of sediment transport on continental shelves. *Marine Modelling,* Vol. 6, *The Sea,* E. D. Coldberg et al. Eds., Wiley and Sons, 539–578.

Speziale, C. G., 1991: Analytical methods for the development of Reynolds-stress closures in turbulence. *Annu. Rev. Fluid Mech.,* **23,** 107–157.

Tolman, H. L., 1994: Wind waves and moveable-bed bottom friction. *J. Phys. Oceanogr.,* **24,** 994–1009.

Townsend, A. A., 1972: Flow in a deep turbulent boundary layer over a surface distorted by water waves. *J. Fluid Mech.,* **55,** 719–735.

——, 1976: *The Structure of Turbulent Shear Flow.* Cambridge University Press, 429 pp.

Trowbridge, J., and O. S. Madsen, 1984: Turbulent wave boundary layers. I. Model formulation and first-order solution. *J. Geophys. Res.,* **89** (C5), 7987–7997.

Van Doorn, T., 1982: experimenteel onderzoek naar het snelheidsveld in de turbulente bodemgrenslaag in een oscillerende stroming in een golftunnel. Delft Hydraulics Laboratory Rep. M1562-1b, Delft, Netherlands.

Weber, S. L., 1991: Bottom friction for wind sea and swell in extreme depth-limited situations. *J. Phys. Oceanogr.,* **21,** 149–172.

Young, I. R., and R. M. Gorman, 1995: Measurements of the evolution of ocean wave spectra due to bottom friction. *J. Geophys. Res.,* **100** (C6), 10 987–11 004.

Zou, Q.-P., 1995: A viscoelastic model for turbulent flow over an undulating topography and progressive waves. Ph.D. thesis, Scripps Institution of Oceanography, 91 pp.

——, 1998: A viscoelastic model for turbulent flow over an undulating topography. *J. Fluid Mech.,* **355,** 81–114.